Progress In Electromagnetics Research, PIER 83, 413–434, 2008

A NOVEL METHOD FOR MICROWAVE BREAST CANCER DETECTION

H. Zhang, S. Y. Tan, and H. S. Tan

School of Electrical and Electronic Engineering
Nanyang Technological University
Block S1, Nanyang Avenue, 639798, Singapore

Abstract—This paper presents a novel method for microwave breast cancer detection using a parallel-plate waveguide probe. The method is based on detecting the dielectric contrast between a malignant tumor and its surrounding tissues. Our analysis and simulations indicate that scattered signals from a tumor (modelled as a lossy dielectric sphere with higher dielectric constant than the surrounding tissues) received in the form of S parameter S_{11} have resonating characteristics in the frequency range of 1 to 7 GHz. A frequency scan of the resonant scattered signals provides data of the presence and location of the tumor. Through numerical examples, the effectiveness of the proposed methodology to detect breast tumors of different sizes, embedded at different depths and to distinguish a tumor from clutter items is demonstrated.

1. INTRODUCTION

Breast cancer being one of the most frequent form of cancer, is the leading cause of cancer deaths in women worldwide [1]. Reduction in mortality rates for cancer deaths can be made possible if cancers are detected and treated early. Thus the role of cancer screening has become increasingly important leading to a demand in effective diagnostic measures; in particular non-invasive cancer diagnostics. Mammography, the gold standard of breast cancer detection requires medical expertise to accurately diagnose the presence of tumor. The number of cancers found with mammography alone is very much less than that found with both mammography and physical examination [2]. Other limitations include having high false negative and false positive rates [3, 4]. Such large false negative and false positive rates lead to increased healthcare cost, unnecessary

medical procedures, and the distress and anxiety on the part of the patient. Other important concerns also include the discomfort due to breast compression and ionizing radiation exposure patients undergo. Therefore there is a need for a new reliable diagnostic technique for breast cancer.

Cancer diagnostics using microwave scattering and reflection has gained significant attention recently. This method is attractive as it is non-invasive and is cheaper and less cumbersome than other screening techniques such as MRI (Magnetic resonance imaging) and PET (Positron emission tomography) [5, 6]. The detection technique is based on the contrast in the electrical properties between a healthy tissue and malignant tumors [7–10]. The major imaging methods proposed based on this approach include ultrawideband (UWB) radar-based system [11–18] and microwave tomography [19–23]. Imaging modality using microwave tomography is even proposed for non-invasive assessments of superficial tissues, and circulatory and excretory systems of the human body [24–27]. Methods of characterization for breast tumors are also investigated. A method for shape and size classifications of the tumor based on signal-to-noise ratios derived from UWB backscatter is available [28]; while in [29] a fast algorithm MIM-SDFMM is utilized to obtain the spectra of tumor which depends on its physical characteristics; and a reconstruction algorithm is also presented in [30] to simultaneously estimate the shape and location of the breast tumor. Complex natural responses (CNR) extraction [31] is also used to identify tumors.

Performing signal processing techniques such as phase correlations in methods such as UWB radar-based system to determine the presence and position of a tumor may not be accurate. As the tissue medium is frequency dispersive, the ultrawideband pulses sent and received differ significantly. In addition, the algorithms to construct the image of the scanned breast, especially using the tomographic methods, require complex and rigorous computations and processing. Furthermore, due to increased complexity, most of the studies conducted on the radar-based system considered only two-dimensional analysis, analyzing three-dimensional imaging models are few and far between [10, 15–18].

In this paper, we propose a novel method using a parallel-plate waveguide probe for S_{11} measurements. The working principle is based on detecting the dielectric contrast between a breast tumor and the surrounding healthy tissue. This method identifies the presence of a tumor in breast tissue by performing contact measurements at different microwave frequencies. The presence of a tumor will alter the reflection coefficients. The greater the contrast in the dielectric properties between a tumor and the surrounding healthy tissue, the

greater is the contrast in the coefficient measured. Additionally, in the presence of any tumor, the backscattered signal received at the aperture of the parallel-plate waveguide probe will display resonance. A frequency scan of the magnitude of the resonant backscattered signal may be used to differentiate between a tumor and clutter items having a much lower dielectric contrast.

The remainder of the paper is organized as follows. Section 2 presents the description of the probe and the derivations of the fields, including the scattered signals from the tumor based on Mie theory [32–34]. In Section 3, an account of the detection method is given. Subsequently in Section 4, numerical results are presented to illustrate the effectiveness of this method. Finally, the conclusions are summarized in Section 5.

2. THEORY AND FORMULATION

The parallel-plate waveguide probe (see Fig. 1) is essentially a transverse electric and magnetic (TEM) mode-excited, cut-off section of a transmission line terminated by ground planes. To simplify analysis, we consider the probe of width $2a$ is infinite in extent in the y-axis, with flanges infinite in extent in both the x- and y-axes.

2.1. Derivation of Radiation Fields

The flanged probe acts as the microwave source radiating into the breast tissue. The radiation fields into a multi-layered dielectric from this flanged guide have been suggested by Lee et al. [35]. We apply this theory for our breast cancer detection method which is based on Mie scattering from a tumor. The scattered signals measured by the parallel-plate waveguide probe depend on the probe's receiving characteristics which we have derived and shown in Section 2.2. The time harmonic variation of $e^{-i\omega t}$ is assumed and suppressed throughout the paper. The incident and reflected magnetic fields inside the parallel-plate waveguide are given respectively as

$$H_y^i(x,z) = H_0^I e^{ik_1 z} \tag{1}$$

$$H_y^r(x,z) = \sum_{m=0}^{\infty} c_m \cos a_m(x+a) e^{-i\xi_m z} \tag{2}$$

where

$$\xi_m = \sqrt{k_1^2 - a_m^2} \tag{3}$$

$$a_m = \frac{m\pi}{2a} \tag{4}$$

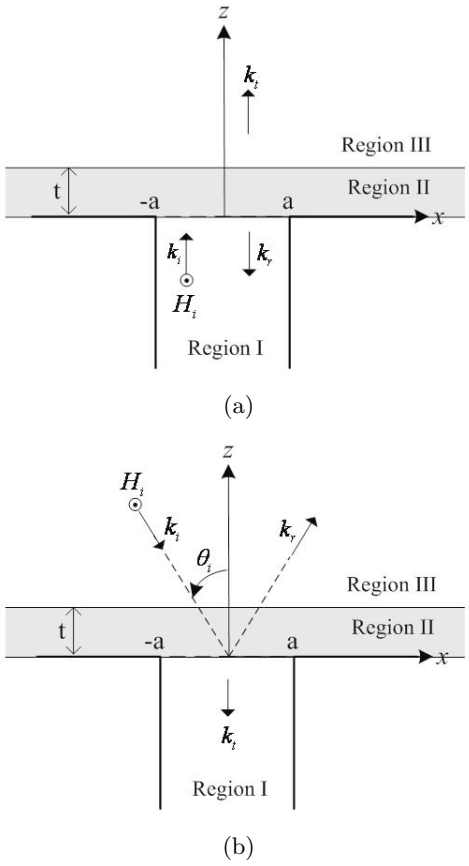

Figure 1. Geometry of the parallel-plate waveguide probe. (a) Radiation from probe. (b) Radiation into probe.

and H_0^I is the amplitude of the incident magnetic field with wavenumber k_1 in the guide (Region I).

The transmitted field outside the probe unbounded in Region III in the spectral domain ζ can be represented as

$$H_y^{III}(x,z) = \frac{1}{2\pi} \int_{-\infty}^{\infty} \tilde{H}_{III}^{+}(\zeta) e^{-i\zeta x + ik_{z_3} z} d\zeta \tag{5}$$

where

$$k_{z_3} = \sqrt{k_3^2 - \zeta^2} \tag{6}$$

$\tilde{H}^{+}_{III}(\zeta)e^{ik_{z_3}t}$ and $H^{III}_{y}(x,t)$ are Fourier transform pair. In the bounded Region II, the field is

$$H^{II}_{y}(x,z) = \frac{1}{2\pi}\int\limits_{-\infty}^{\infty}\left[\tilde{H}^{+}_{II}(\zeta)e^{ik_{z_2}z} + \tilde{H}^{-}_{II}(\zeta)e^{-ik_{z_2}z}\right]e^{-i\zeta x}d\zeta \tag{7}$$

where

$$k_{z_2} = \sqrt{k_2^2 - \zeta^2} \tag{8}$$

k_2 and k_3 are the wave numbers in the Regions II and III respectively.

The boundary conditions require tangential E field continuity in the x-direction and tangential H field continuity at $z = t$. Matching boundary conditions yields

$$\tilde{H}^{-}_{II}(\zeta) = e^{i2k_{z_2}t}\left(\frac{\varepsilon_3 k_{z_2} - \varepsilon_2 k_{z_3}}{\varepsilon_3 k_{z_2} + \varepsilon_2 k_{z_3}}\right)\tilde{H}^{+}_{II}(\zeta) \tag{9}$$

and

$$\tilde{H}^{+}_{III}(\zeta) = e^{i\left(k_{z_2}-k_{z_3}\right)t}\left(1 + \frac{\varepsilon_3 k_{z_2} - \varepsilon_2 k_{z_3}}{\varepsilon_3 k_{z_2} + \varepsilon_2 k_{z_3}}\right)\tilde{H}^{+}_{II}(\zeta). \tag{10}$$

The tangential E field continuity at the aperture $(-a < x < a, z = 0)$ yields

$$\tilde{H}^{+}_{II}(\zeta) = \left(\frac{1}{1-\alpha}\right)\frac{\varepsilon_2}{\varepsilon_1}\left[H^{I}_{0}\xi_0 K_0(\zeta) - \sum_{m=0}^{\infty} c_m \xi_m K_m(\zeta)\right] \tag{11}$$

where

$$\alpha = e^{i2k_{z_2}t}\left(\frac{\varepsilon_3 k_{z_2} - \varepsilon_2 k_{z_3}}{\varepsilon_3 k_{z_2} + \varepsilon_2 k_{z_3}}\right) \tag{12}$$

$$K_m(\zeta) = \frac{-i\zeta}{k_{z_2}\left(\zeta^2 - a_m^2\right)}\left[e^{i\zeta a}(-1)^m - e^{-i\zeta a}\right]. \tag{13}$$

Subsequently, the tangential H field continuity in the aperture plane yields

$$\begin{aligned}&\frac{1}{2\pi}\int\limits_{-\infty}^{\infty}\left(\frac{1+\alpha}{1-\alpha}\right)\frac{\varepsilon_2}{\varepsilon_1}\left[H^{I}_{0}\xi_0 K_0(\zeta) - \sum_{m=0}^{\infty} c_m \xi_m K_m(\zeta)\right]e^{-i\zeta x}d\zeta \\ &= H^{I}_{0} + \sum_{m=0}^{\infty} c_m \cos a_m(x+a).\end{aligned} \tag{14}$$

Multiplying (14) by $\cos a_n(x+a)$ and integrating both sides with respect to x from $-a$ to a, one obtains

$$\frac{\varepsilon_2}{\varepsilon_1}\left[H_o^I\xi_0 J_{0n} - \sum_{m=0}^{\infty}\xi_m c_m J_{mn}\right] = 2\pi a\left(H_0^I\delta_{n0} + c_n\right)\psi_n \tag{15}$$

where δ_{mn} represents the Kronecker delta, $\psi_0 = 2,\ \psi_1 = \psi_2 = \cdots = 1$, and

$$J_{mn} = \int_{-\infty}^{\infty}\left(\frac{1+\alpha}{1-\alpha}\right)\frac{\zeta^2\left[(-1)^m e^{i\zeta a} - e^{-i\zeta a}\right]\left[(-1)^n e^{-i\zeta a} - e^{i\zeta a}\right]}{k_{z_2}\left(\zeta^2 - a_m^2\right)\left(\zeta^2 - a_n^2\right)}d\zeta. \tag{16}$$

Solving for the unknown coefficients c_m and substituted into (10) to evaluate $\tilde{H}_{III}^{+}(\zeta)$ yields the x-direction electric field E_x^{III} and z-direction electric field E_z^{III} in Region III respectively as

$$E_x^{III}(x,z) = \frac{1}{2\pi}\int_{-\infty}^{\infty}\frac{k_{z_3}}{\omega\varepsilon_3}\tilde{H}_{III}^{+}(\zeta,0)e^{-i\zeta x + ik_{z_3}z}d\zeta \tag{17}$$

$$E_z^{III}(x,z) = \frac{1}{2\pi}\int_{-\infty}^{\infty}\frac{\zeta}{\omega\varepsilon_3}\tilde{H}_{III}^{+}(\zeta,0)e^{-i\zeta x + ik_{z_3}z}d\zeta. \tag{18}$$

In addition, the reflection coefficient (for healthy tissues without any tumor) at the aperture of the probe Γ_0 is given by

$$\Gamma_0(\omega) = \frac{E_x^r}{E_x^i} = -\frac{c_0}{H_0^I} \tag{19}$$

where E_x^i and E_x^r are the incident and reflected electric fields at the aperture respectively, and c_0 is the amplitude of the dominant mode reflected magnetic field in Region I.

2.2. Derivation of Transmitted Fields into the Probe

With a plane wave at oblique incidence into the probe, the incident and reflected magnetic fields in Region III are given respectively as (see Fig. 1(b))

$$H_y^i(x,z) = H_0^{III}e^{ik_x x - ik_z(z-t)} \tag{20}$$

$$H_y^r(x,z) = \frac{1}{2\pi}\int_{-\infty}^{\infty}\tilde{H}_{III}^{+}(\zeta)e^{-i\zeta x + ik_{z_3}(z-t)}d\zeta, \tag{21}$$

while the field in the bounded Region II is given as

$$H_y^{II}(x,z) = \frac{1}{2\pi}\int_{-\infty}^{\infty}\left[\tilde{H}_{II}^{+}(\zeta)e^{ik_{z_2}z} + \tilde{H}_{II}^{-}(\zeta)e^{-ik_{z_2}z}\right]e^{-i\zeta x}d\zeta \tag{22}$$

and the transmitted field inside the waveguide can be represented as

$$H_y^{t}(x,z) = \sum_{m=0}^{\infty} b_m \cos a_m(x+a)e^{-i\xi_m z} \tag{23}$$

where

$$k_x = k_3 \sin\theta_i \tag{24}$$

$$k_z = k_3 \cos\theta_i \tag{25}$$

and H_0^{III} is the amplitude of the incident magnetic field in Region III; k_1, k_2, k_3, k_{z_2}, k_{z_3}, ξ_m, a_m are as previously defined.

Matching the boundary continuities of tangential E field and tangential H field is required to determine the unknown coefficients b_m. The tangential E and H field continuities at $z = t$ yields

$$\tilde{H}_{II}^{-}(\zeta) = \alpha\tilde{H}_{II}^{+}(\zeta) + 2\pi H_0^{III}\beta\delta(\zeta - k_x) \tag{26}$$

where

$$\beta = e^{ik_{z_2}t}\left(\frac{\varepsilon_2(k_{z_3}+k_z)}{k_{z_2}\varepsilon_3 + k_{z_3}\varepsilon_2}\right) \tag{27}$$

δ denotes the Dirac delta function and α takes the form of (12).

Following, the tangential E field continuity at the aperture ($-a < x < a, z = 0$) yields

$$\tilde{H}_{II}^{+}(\zeta) = \frac{1}{1-\alpha}\left\{\left[2\pi H_0^{III}\beta\delta(\zeta - k_x)\right] - \frac{\varepsilon_2}{\varepsilon_1}\sum_{m=0}^{\infty} b_m\xi_m K_m(\zeta)\right\}. \tag{28}$$

Subsequently tangential H field continuity at the aperture gives

$$\begin{aligned}&\sum_{m=0}^{\infty} b_m \cos a_m(x+a)e^{-i\xi_m z} = \\ &\frac{1}{2\pi}\int_{-\infty}^{\infty}\left\{(1+\alpha)\tilde{H}_{II}^{+}(\zeta) + \left[2\pi H_0^{III}\beta\delta\left(\zeta - k_x\right)\right]\right. \\ &\left.-\frac{\varepsilon_2}{\varepsilon_1}\sum_{m=0}^{\infty} b_m\xi_m K_m(\zeta)\right\}e^{-i\zeta x}d\zeta.\end{aligned} \tag{29}$$

Multiplying (29) by $\cos a_n(x+a)$ and integrating both sides with respect to x from $-a$ to a, with the use of time-delayed Dirac delta property [36], one obtains

$$\sum_{m=0}^{\infty} \frac{\varepsilon_2}{\varepsilon_1} \xi_m b_m J_{mn} = 2\pi \left(\frac{4H_0^{II} \varepsilon_2 k_z}{\varepsilon_3 \sqrt{k_2^2 - k_x^2} + \varepsilon_2 k_z - e^{i2k_{z_2}t} \left(\varepsilon_3 \sqrt{k_2^2 - k_x^2} + \varepsilon_2 k_z \right)} L_n - a\psi_n b_n \right) \quad (30)$$

where

$$L_n = \frac{ik_x \left[(-1)^n e^{ik_x a} - e^{-ik_x a} \right]}{a_n^2 - k_x^2} \quad (31)$$

$\psi_0 = 2,\ \psi_1 = \psi_2 = \cdots = 1$, and J_{mn} takes the form of (16).

If D is the determinant of the system of $M+1$ linear equations in (30), and $M+1$ is the number of modes to be taken into consideration, the elements b_m can be solved by applying the Cramer's Theorem [37]

$$b_0 = \frac{D_1}{D},\ b_1 = \frac{D_2}{D},\ \cdots,\ b_M = \frac{D_{M+1}}{D} \quad (32)$$

where D_k is the determinant obtained from D by replacing D the kth column by the column with the $N+1$ elements on the right hand side of (30).

The transmission coefficient at the aperture of the probe τ_0 can then be derived as

$$\tau_0(\omega) = \frac{E^t}{E^i} = \frac{b_0}{H_0^{III}} \quad (33)$$

where E^i and E^t are the incident and transmitted (or received) electric fields at the aperture respectively, b_0 is the amplitude of the dominant mode transmitted magnetic field in Region I.

2.3. Scattering Characteristics

The detection technique is based on the Mie scattering of a dielectric body [33, 34, 38]. Consider a small spherical tumor of radius r_0, embedded at (x_0, z_0) in Fig. 2. To simplify the analysis, the field incident onto the small tumor is assumed to be locally plane. The exact solution for plane wave scattering by a homogeneous sphere (Mie scattering [33]) is as follows.

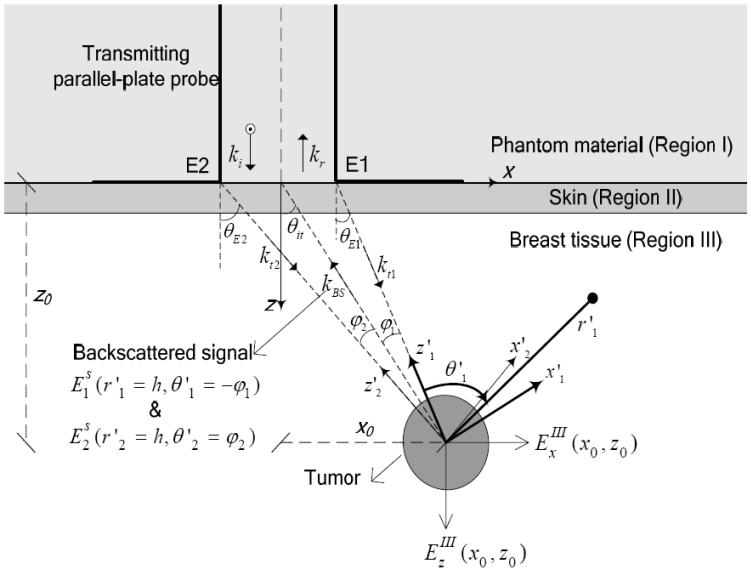

Figure 2. Vertical cross-sectional view of a parallel-plate waveguide probe radiating into a breast tissue and receiving the backscattered signal from the tumor.

Consider a plane wave polarized in the x_1'-direction moving in the negative z_1'-direction, with expression

$$\boldsymbol{E}^{inc} = E_o \hat{a}_{x_1'} e^{-ik_3 z_1'}. \tag{34}$$

The scattered electric field at a point $P\ (r_1', \theta_1', \phi_1')$ outside the sphere, is given by

$$\boldsymbol{E}^s(P,\omega) = E_o \frac{e^{ik_3 r_1'}}{k_3 r_1'} \left[\cos\phi_1' S_1(\theta_1')\hat{a}_{\theta_1'} - \sin\phi_1' S_2(\theta_1')\hat{a}_{\phi_1'}\right] \tag{35}$$

where

$$S_1(\theta_1') = \sum_{n=1}^{\infty} (-i)^{n+1} \left[A_n \frac{P_n^1(\cos\theta_1')}{\sin\theta_1'} + iB_n \frac{d}{d\theta_1'} P_n^1(\cos\theta_1')\right] \tag{36}$$

and

$$S_2(\theta_1') = \sum_{n=1}^{\infty} (-i)^{n+1} \left[A_n \frac{d}{d\theta_1'} P_n^1(\cos\theta_1') + iB_n \frac{P_n^1(\cos\theta_1')}{\sin\theta_1'}\right]. \tag{37}$$

Denoting the medium of the sphere with a wave number

$$k_4 = \omega\sqrt{\varepsilon_4\mu_0} = \omega\sqrt{(\varepsilon_4' + i\varepsilon_4'')\mu_0} = k_3 m_4, \tag{38}$$

the coefficients of the Mie solution are given by

$$A_n = (-i)^n \frac{2n+1}{n(n+1)} \left[\frac{j_n(k_3r_0)[k_4r_0 j_n(k_4r_0)]' - j_n(k_4r_0)[k_3r_0 j_n(k_3r_0)]'}{j_n(k_4r_0)[k_3r_0 h_n^{(1)}(k_3r_0)]' - h_n^{(1)}(k_3r_0)[k_4r_0 j_n(k_4r_0)]'}\right] \tag{39}$$

$$B_n = (-i)^{n+1} \frac{2n+1}{n(n+1)} \left[\frac{j_n(k_3r_0)[k_4r_0 j_n(k_4r_0)]' - m_4^2 j_n(k_4r_0)[k_3r_0 j_n(k_3r_0)]'}{h_n^{(1)}(k_3r_0)[k_4r_0 j_n(k_4r_0)]' - m_4^2 j_n(k_4r_0)[k_3r_0 h_n^{(1)}(k_3r_0)]'}\right]. \tag{40}$$

The primes, $[\,]'$, denote differentiation with respect to the argument k_3r_0 or k_4r_0. For the special case of backscattering ($\theta_1' = 0$), the result simplifies to [34]

$$E^s\left(r_1', \theta_1' = 0, \omega\right) = E_o \frac{e^{ik_3r_1'}}{k_3 r_1'} \sum_{n=1}^{\infty} (-i)^{n+1} \frac{n(n+1)}{2} \left[A_n + iB_n\right] \tag{41}$$

It can be proved from uniform geometrical theory of diffraction (UTD) that a field point in Region III is illuminated by the fields diffracted from the edges of the parallel-plate waveguide probe at E1 and E2 respectively (see Fig. 2) [39, 40]. Hence it is possible to resolve the incident fields at the tumor, $E_x^{III}(x_0, z_0)$ and $E_z^{III}(x_0, z_0)$, into components of plane wave emanating from the two edges E1 and E2; thus resulting in two contributions of the scattered electric field. By superposition, the effective scattered signals can be found.

In the presence of a tumor, the reflection coefficient Γ_t, or the backscattered signal in S_{11} measured at the aperture of the parallel-plate waveguide probe would thus be expressed as

$$\Gamma_t = \frac{E_x^r + \tau_0\left(E_1^s + E_2^s\right)}{E_x^i} = \Gamma_0 + \Delta\Gamma \tag{42}$$

where

$$\Delta\Gamma = \frac{\tau_0\left[E_1^s(r_1' = h, \theta_1' = \varphi_1, \omega) + E_2^s(r_2' = h, \theta_2' = \varphi_2, \omega)\right]}{E_x^i}, \tag{43}$$

$$h = \sqrt{x_0^2 + z_0^2} \tag{44}$$

$$\theta_{it} = \tan^{-1}\left(\frac{x_0}{z_0}\right) \tag{45}$$

$$\varphi_1 = \theta_{it} - \theta_{E1} \tag{46}$$

$$\varphi_2 = \theta_{E2} - \theta_{it}. \tag{47}$$

And E_x^i is the incident field; $E_1^s\,(r_1' = h,\ \theta_1' = \varphi_1, \omega)$ and $E_2^s\,(r_2' = h,\ \theta_2' = \varphi_2, \omega)$ are the backscattered fields at the aperture of the transmitting probe respectively, due to the presence of the tumor. The probe characteristic τ_0 is dependent on the angle θ_{it}, and can be derived using (30).

For simplicity of analysis, the scattered electric field from the scatterer is assumed to be plane wave.

3. METHODOLOGY

Measurements for breast cancer detection can be done at a range of microwave frequencies using the parallel-plate waveguide probe, with a vector network analyzer to measure the S parameter S_{11}. The parallel-plate waveguide probe is designed for only the dominant mode waves to propagate in the 1 to 7 GHz range. To minimize reflections which can arise due to interfaces between different mediums, the probe is to be immersed in a liquid phantom material of known properties [41], in this case skin-mimicking phantom is selected.

Measurements of S_{11} are taken at different positions of the probe in contact with the tissue (see Fig. 3). The difference in each pair of the measurements of S_{11} can be used to determine the presence and size of the tumor. With N measurements at different positions of the breast, there can be ${}^{N}\mathrm{C}_2$ pairs of differences in backscattered signals or S_{11} measured. $\Delta\Gamma$, the difference in S_{11} contained in each pair, is dependent on the receiving characteristic of the probe τ_0. This difference contains information on the backscattered signal from the scatterer (if any). In the presence of a tumor, the backscattered signal will have resonant characteristics with respect to frequency and amplitude, whereas in a frequency scan the backscattered signal from healthy tissue will not contain any resonant features. No presence of tumor at the positions where the two measurements are made is indicated by an absence of resonant characteristic in $\Delta\Gamma$. If there is a resonating response, then one of the signals measured by the probe contains the backscattered signal from the tumor. The final position of the tumor can thus be predicted by eliminating the positions with no tumor. Further to this, the resonant backscattered signals and their magnitudes may be used to differentiate between a tumor and clutter items. Apart from surveying the entire breast surface with one

probe, the detection principle can be extended to having an array of the parallel- plate waveguide probes arranged to accommodate the shape of the breast.

4. NUMERICAL RESULTS AND DISCUSSIONS

Numerical simulations have been conducted to verify the performance of the proposed technique. Consider a spherical tumor of diameter d_0 embedded in the breast with a skin layer of 2 mm thickness [42] (modelled as a concentric hemisphere of radius 50 mm) at a depth h from the surface in Fig. 3. The breast and the probe are immersed in a phantom material. In the simulations only the first order scattering from the scatterer is taken into account.

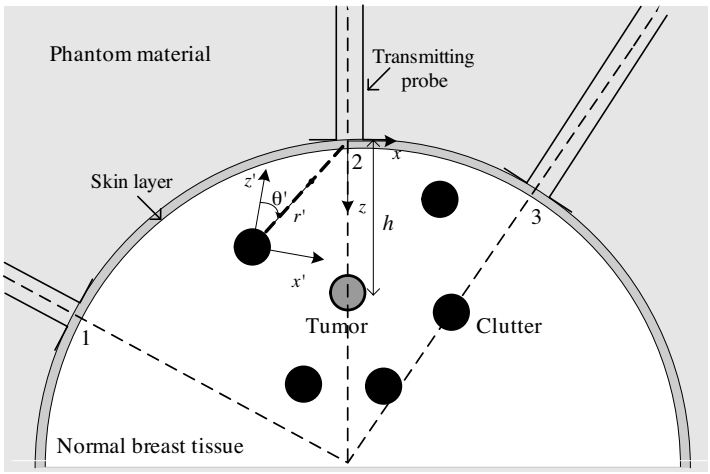

Figure 3. Parallel-plate waveguide probe at different positions of the breast tissue for S_{11} measurements.

In this paper, a two-pole Debye dispersion equation [12] is employed to model the frequency dependence of the dielectric properties

$$\varepsilon_r(\omega) - j\frac{\sigma(\omega)}{\omega\varepsilon_0} = \varepsilon_\infty + \sum_{p=1}^{2} \frac{\varepsilon_{sp} - \varepsilon_\infty}{1 + j\omega\tau_p} \tag{48}$$

where ε_0 is the free space permittivity, ω is the angular frequency. The following assumptions are made in the simulations. The parallel-plate waveguide probe is designed to have a next higher order mode cut-off

frequency of more than 7 GHz, e.g., for a probe (width $2a = 6$ mm) filled with phantom material simulating a normal breast tissue, the next higher order mode cut-off frequency is about 7.8 GHz. The following Debye parameters are used to fit data for the breast tissue for the entire swept frequency range: normal tissue ($\varepsilon_\infty = 2.68, \varepsilon_{s1} = 5.01$, $\varepsilon_{s2} = 3.85$, $\tau_1 = 15.84$ ps, $\tau_2 = 0.10$ ns), malignant tissue ($\varepsilon_\infty = 11.05$, $\varepsilon_{s1} = 51.67$, $\varepsilon_{s2} = 43.35$, $\tau_1 = 8.56$ ps, $\tau_2 = 0.23$ ns) and skin layer ($\varepsilon_\infty = 4.62$, $\varepsilon_{s1} = 37.10$, $\varepsilon_{s2} = 41.22$, $\tau_1 = 7.51$ ps, $\tau_2 = 0.31$ ns) [12]. Clutter item that represents tissue heterogeneity, having dielectric properties of variation of +30% that of the normal tissue is included in the breast model used [14].

Assuming three backscattered measurements are made (see Fig. 3), given as Γ_1 (reflection coefficient detected at position 1), Γ_2 (reflection coefficient detected at position 2), and Γ_3 (reflection coefficient detected at position 3). There are 5 clutter items surrounding the tumor. With reference to coordinate system at position 2 as shown in Fig. 3, the clutter item 1 is at ($x = 6$ mm, $z = 39$ mm); clutter item 2 is at ($x = 15$ mm, $z = 24$ mm); clutter item 3 is at ($x = 12$ mm, $z = 9$ mm); clutter item 4 is at ($x = -10$ mm, $z = 15$ mm); clutter item 5 is at ($x = -10$ mm, $z = 40$ mm); and the tumor is located at ($x = 0$, $z = 20$ mm). Three readings available will result in three ($^3C_2$) combinations of differences: $\Delta\Gamma_{21}$ (between Γ_1 and Γ_2); $\Delta\Gamma_{23}$ (between Γ_2 and Γ_3) and $\Delta\Gamma_{31}$ (between Γ_1 and Γ_3). It is assumed that there is no interaction between the tumor and clutters. The three $\Delta\Gamma$ are plotted as follows.

Figure 4(a) shows the plots of the magnitude of the difference in the reflection coefficients Γ_2 and Γ_1, $\Delta\Gamma_{21}$; and difference in Γ_2 and Γ_3, $\Delta\Gamma_{23}$ display resonance at the frequencies 5.0 GHz and 4.6 GHz respectively. Γ_2, the reflection coefficient measured at position 2, containing the strongest backscatter signal from the tumor is present in both $\Delta\Gamma$. Additionally, it is noted that the amplitude of the difference $\Delta\Gamma_{31}$ (between Γ_3 and Γ_1) displays no obvious resonance and is about 5 times lower than the amplitude of $\Delta\Gamma_{21}$ and $\Delta\Gamma_{23}$. In terms of power, the difference in the magnitude of $\Delta\Gamma$ at resonance gives a factor of about 25 times. Hence this factor can be used to predict the location of the tumor; one can predict a tumor is embedded around position 2. Also, the summation of the magnitudes of the three difference in reflection coefficients $\Sigma\Delta\Gamma(\Delta\Gamma_{21} + \Delta\Gamma_{23} + \Delta\Gamma_{31})$ shows a very clear resonance at 4.8 GHz with resonant amplitude of 2.2×10^{-2}. In Fig. 4(b), where the tumor is replaced by a clutter item of the same size, it is noted that there is no clear resonance in both $\Delta\Gamma$ and $\Sigma\Delta\Gamma$. The amplitude of $\Sigma\Delta\Gamma$ due to all clutter items is more than 10 times lower that the resonant amplitude of $\Sigma\Delta\Gamma$ in Fig. 4(a).

This is essential for differentiating between the presence of a tumor or the presence of clutter of the same size. As tumors have much higher dielectric contrast to the surrounding healthy tissue than clutter, it will backscatter larger power. The difference in resonant amplitudes therefore can be used as a tool to differentiate between a tumor and clutter items.

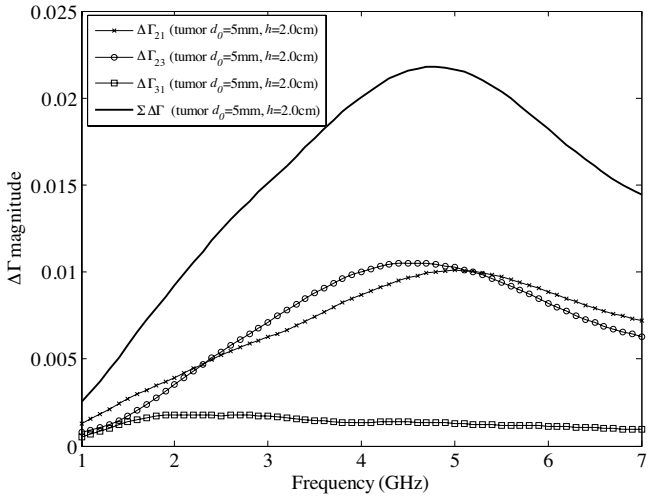

(a)

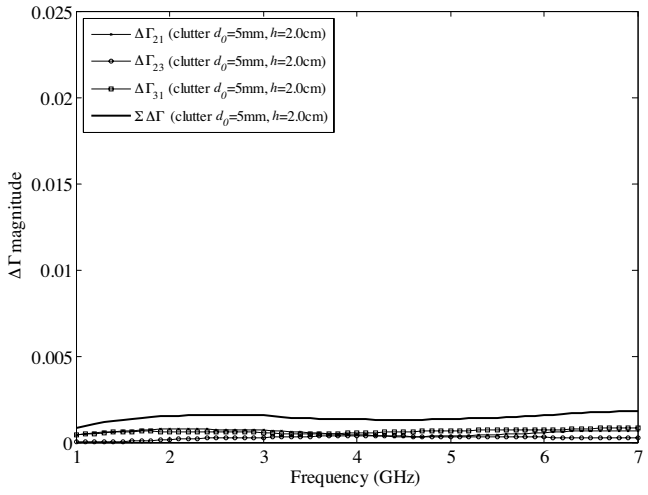

(b)

Figure 4. Magnitude of the differences in the reflection coefficients $\Delta\Gamma$. (a) 1 tumor surrounded by 5 clutter items. (b) All 6 clutter items.

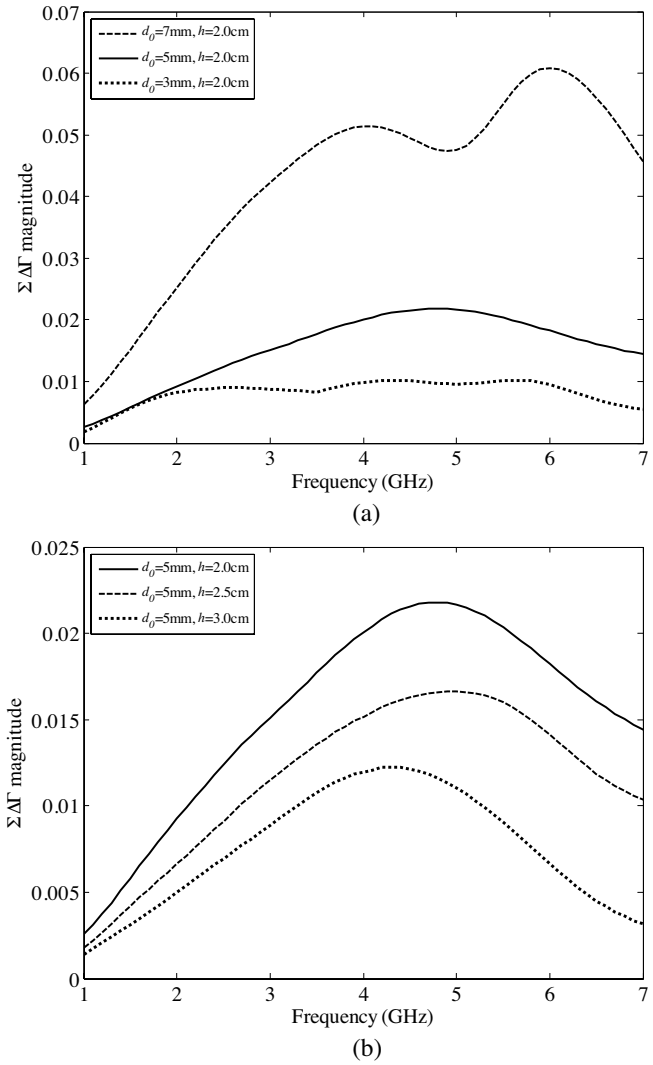

Figure 5. Comparison of $\Sigma\Delta\Gamma$, the summation of the magnitude of the differences in the reflection coefficients for (a) Tumor of different sizes. (b) Tumor at different depths.

In general, larger scatterers (tumor or clutter) result in larger backscattered power. This is observed in Fig. 5(a) where the summation of the magnitudes of the various differences in reflection coefficients at different positions $\Sigma\Delta\Gamma$ due to a tumor of a larger diameter of 7 mm is greater than that by a tumor of smaller diameters

of 5 mm or 3 mm. Furthermore, in Fig. 5(b) a comparison of $\Sigma\Delta\Gamma$ whereby the tumor is embedded at $h = 20\,\text{mm}$, $h = 25\,\text{mm}$ or $h = 30\,\text{mm}$ shows that the resonant frequency is about 4.8 GHz. It is not much affected by the depth of the tumor in the tissue.

It is shown in Fig. 5(b) that there is a difference of about 2.4 dB in the magnitudes of $\Sigma\Delta\Gamma$ at resonant frequency of 4.8 GHz for a tumor of $d_0 = 5\,\text{mm}$ embedded at different depths of 2.0 cm and 2.5 cm ($\Sigma\Delta\Gamma_{h=2.0\,\text{cm},\ 4.8\,\text{GHz}} = -33.2\,\text{dB}$, $\Sigma\Delta\Gamma_{h=2.5\,\text{cm},\ 4.8\,\text{GHz}} = -35.6\,\text{dB}$). This difference in the scattered power at resonance can be accounted for by considering the absorption loss in the breast tissue and the spreading losses from the probe to the tumor and backscattered to the probe with this total loss given as

$$\text{Total Loss} = 0.5 \times \left[20 \log_{10} \left(\frac{h_1}{h_2} \right)^{3/2} + 2(h_1 - h_2)\alpha \right] \tag{49}$$

where h_1 and h_2 are the different depths the tumor is embedded.

The radiated wave from the transmitting probe can be shown to have an approximately cylindrical wavefront, whereas the wavefront of the scattered signal from the spherical tumor is approximately spherical. Using (48), the attenuation constant α is found to be approximately 2.51 dB/cm at 4.8 GHz. The additional spreading loss and absorption loss due to the increased depth from 2.0 cm to 2.5 cm is thus given by 1.45 dB and 1.25 dB respectively. Therefore the total loss in resonant $\Sigma\Delta\Gamma$ at 4.8 GHz is 2.7 dB, which agrees with the observations. Similarly, the total loss in $\Sigma\Delta\Gamma$ at resonant frequency when the tumor is embedded at $h = 30\,\text{mm}$ can be accounted for by the same procedure: additional spreading loss and absorption loss due to the increased depth from 2.0 cm to 3.0 cm is given by by 2.64 dB and 2.38 dB respectively; hence it can be predicted that the resonant amplitude of $\Sigma\Delta\Gamma$ for the tumor embedded at $h = 30\,\text{mm}$ is 5.0 dB smaller than that for a tumor embedded at $h = 20\,\text{mm}$. This tallies with the observations from Fig. 5(b) as it is noted that $\Sigma\Delta\Gamma_{h=2.0\,\text{cm},\ 4.8\,\text{GHz}} = -33.2\,\text{dB}$ and $\Sigma\Delta\Gamma_{h=3.0\,\text{cm},\ 4.6\,\text{GHz}} = -38.2\,\text{dB}$.

5. CONCLUSIONS AND FUTURE WORK

A novel method using parallel-plate waveguide probes is proposed for non-invasive breast cancer detection. The basis for this method is provided by detecting the dielectric contrast between normal breast tissue and a tumor or other tissue heterogeneity (clutter) to determine the presence of a tumor. A tumor scatters the signal radiated from the probe; and the backscattered signals received in the form of

S_{11} have resonating characteristics. Within the assumption of there exists a large contrast between a tumor and its surrounding tissues, numerical simulations have also shown that this technique is effective in distinguishing a tumor from clutter. However a recent large scale study of dielectric properties of normal, benign and malignant breast tissues samples in the ultrawideband microwave frequency range of 0.5–20 GHz, obtained from reduction and cancer surgeries [43, 44] shows that the dielectric contrast in the between malignant and normal glandular/fibroconnective tissues in the breast may be no more than about 10%. The effectiveness and robustness of this proposed method would be further investigated using the properties reported in these literatures [43–45]. Furthermore, scattering characteristics for an ellipsoidal tumor would be subsequently analyzed [46].

Structural variations to the parallel-plate waveguide probe for shaping radiation for more precise localization of tumor and to reduce radiation leakages would also be addressed in future.

The theory and formulations proposed are not restricted to biomedical imaging of tumors but can also be extended to applications in detecting concealed objects such as landmines, metallic pipes hidden in concrete, etc. [47–49]. It only requires knowledge of the electrical properties of the object and its surrounding media such as complex permittivity and permeability, and morphological properties such as the shape, to modify our design for detection.

ACKNOWLEDGMENT

Author Zhang Huiyu thankfully acknowledge the Agency for Science, Technology and Research (A*STAR) of Singapore for providing A*STAR Graduate Scholarship.

REFERENCES

1. World Health Organization Fact Sheet No. 297: Cancer (February 2006) [Online]. Available: http://www.who.int/mediacentre/factsheets/fs297/en/index.html
2. Huynh, P. T., A. M. Jarolimek, and S. Daye, "The false-negative mammogram," *Radiographics*, Vol. 18, 1137–1154, 1998.
3. Fletcher, S. W. and J. G. Elmore, "Mammographic screening for breast cancer," *New Engl. J. Med.*, Vol. 37, 1672–1680, 2003.
4. Fear, E. C., P. M. Meaney, and M. A. Stuchly, "Microwaves for breast cancer detection," *IEEE Potentials*, Vol. 22, No. 1, 12–18, February–March 2003.

5. Moore, S. K., "Better breast cancer detection," *IEEE Spectrum*, Vol. 38, No. 5, 50–54, May 2001.
6. Fear, E. C., "Microwave imaging of the breast," *TCRT*, Vol. 4, No. 1, 69–85, February 2005.
7. Bindu, G., S. J. Abraham, A. Lonappan, V. Thomas, C. K. Aanandan, and K. T. Mathew, "Active microwave imaging for breast cancer detection," *Progress In Electromagnetics Research*, PIER 58, 149–169, 2006.
8. Fear, E. C., S. C. Hagness, P. M. Meaney, M. Okoniewski, and M. A. Stuchly, "Enhancing breast tumor detection with near field imaging," *IEEE Microw. Mag.*, Vol. 3, No. 1, 48–56, March 2002.
9. Fear, E. C. and M. A. Stuchly, "Microwave detection of breast cancer," *IEEE Trans. Microw. Theory Tech.*, Vol. 48, No. 11, Part 1, 1854–1863, November 2000.
10. Guo, B., Y. Wang, and J. Li, "Active imaging via adaptive beamforming methods for breast cancer detection," *Journal of Electromagnetic Waves and Applications*, Vol. 20, No. 1, 53–63, 2006.
11. Davis, S. K., E. J. Bond, S. C. Hagness, and B. D. Van Veen, "Microwave imaging via space-time beamforming for early detection of breast cancer: Beamformer design in the frequency domain," *Journal of Electromagnetic Waves and Applications*, Vol. 17, No. 2, 357–381, 2003.
12. Lim, H. B., T. T. N. Nguyen, E. Li, and D. T. Nguyen, "Confocal microwave imaging for breast cancer detection: Delay-multiply-and-sum image reconstruction algorithm," *IEEE Trans. Biomed. Eng.*, Vol. 55, No. 6, 1697–1704, June 2008.
13. Chen, Y., E. Gunawan, K. S. Low, S. Wang, C. B. Soh, and L. L. Thi, "Time of arrival data fusion method for two-dimensional ultrawideband breast cancer detection," *IEEE Trans. Antennas Propag.*, Vol. 55, No. 10, 2852–2865, October 2007.
14. Chen, Y., E. Gunawan, K. S. Low, S. Wang, Y. Kim, and C. B. Soh, "Pulse design for time reversal method as applied to ultrawideband microwave breast cancer detection: A two-dimensional analysis," *IEEE Trans. Antennas Propag.*, Vol. 55, No. 1, 194–204, January 2007.
15. Xie, Y., B. Guo, L. Xu, J. Li, and P. Stoica, "Multistatic adaptive microwave imaging for early breast cancer detection," *IEEE Trans. Biomed. Eng.*, Vol. 53, No. 8, 1647–1657, August 2006.
16. Fear, E. C., X. Li, S. C. Hagness, and M. A. Stuchly, "Confocal

microwave imaging for breast cancer detection: Localization of tumors in three dimensions," *IEEE Trans. Biomed. Eng.*, Vol. 49, No. 8, 812–821, August 2002.

17. Kosmas, P. and C. M. Rappaport, "FDTD-based time reversal approach for microwave breast cancer detection — Localization in three dimensions," *IEEE Trans. Microw. Theory Tech.*, Vol. 54, No. 4, 1921–1927, June 2006.
18. Hagness, S. C., A. Taflove, and J. E. Brdiges, "Three-dimensional FDTD analysis of a pulsed microwave confocal system for breast cancer detection: Design of an antenna array element," *IEEE Trans. Antennas Propag.*, Vol. 47, No. 5, 783–791, May 1999.
19. Arunachalam, K., L. Udpa, and S. S. Udpa, "A computational investigation of microwave breast imaging using deformable reflector," *IEEE Trans. Biomed. Eng.*, Vol. 55, No. 2, Part 1, 554–562, February 2008.
20. Semenov, S. Y., R. H. Svenson, A. E. Boulyshev, A. E. Souvorov, A. G. Nazarov, Y. Sizov, V. Posukh, A. Pavlovsky, P. Repin, A. Starostin, B. Voinov, M. Taran, G. Tatsis, and V. Baranov, "Three-dimensional microwave tomography: Initial experimental imaging of animals," *IEEE Trans. Biomed. Eng.*, Vol. 49, No. 1, 55–63, January 2002.
21. Semenov, S. Y, R. H. Svenson, A. E. Boulyshev, A. E. Souvorov, V. Y. Borisov, Y. Sizov, A. N. Starostin, K. R. Dezern, G. P. Tatsis, and V. Y. Baranov, "Microwave tomography: Two-dimensional system for biological imaging," *IEEE Trans. Biomed. Eng.*, Vol. 43, No. 9, 869–877, September 1996.
22. Boulyshev, A. E., S. Y Semenov, A. E. Souvorov, R. H. Svenson, A. G. Nazarov, Y. Sizov, and G. P. Tatsis, "Computational modeling of three-dimensional microwave tomography of breast cancer," *IEEE Trans. Biomed. Eng.*, Vol. 48, No. 9, 1053–1056, September 2001.
23. Semenov, S. Y., A. E. Boulyshev, A. Abubakar, V. G. Posukh, Y. Sizov, A. E. Souvorov, P. M. van den Berg, and T. C. Williams, "Microwave-tomographic imaging of the high dielectric-contrast objects using different image-reconstruction approaches," *IEEE Trans. Microw. Theory Tech.*, Vol. 53, No. 5, 2284–2294, July 2005.
24. Yan, L. P., K. M. Huang, and C. J. Liu, "A noninvasive method for determining dielectric properties of layered tissues on human back," *Journal of Electromagnetic Waves and Applications*, Vol. 21, No. 13, 1829–1843, 2007.
25. Lonappan, A., G. Bindu, V. Thomas, and J. Jacob, "Diagnosis of

diabetes mellitus using microwaves," *Journal of Electromagnetic Waves and Applications*, Vol. 21, No. 10, 1393–1401, 2007.

26. Lonappan, A., V. Thomas, and G. Bindu, "Nondestructive measurement of human blood at microwave frequencies," *Journal of Electromagnetic Waves and Applications*, Vol. 21, No. 8, 1131–1139, 2007.
27. Semenov, S. Y., V. G. Posukh, A. E. Boulyshev, and T. C. Williams, "Microwave tomographic imaging of the heart in intact swine," *Journal of Electromagnetic Waves and Applications*, Vol. 20, No. 7, 873–890, 2006.
28. Davis, S. K., B. D. Van Veen, S. C. Hagness, and F. Kelcz, "Breast tumor characterization based on ultrawideband microwave backscatter," *IEEE Trans. Biomed. Eng.*, Vol. 55, No. 1, 237–246, January 2008.
29. El-Shenawee, M., "Resonant spectra of malignant breast cancer tumors using the three-dimensional electromagnetic fast multipole model," *IEEE Trans. Biomed. Eng.*, Vol. 51, No. 1, 35–44, January 2004.
30. El-Shenawee, M. and E. L. Miller, "Spherical harmonics microwave algorithm for shape and location reconstruction of breast cancer tumor," *IEEE Trans. Med. Imaging*, Vol. 25, No. 10, 1258–1271, October 2006.
31. Huo, Y., R. Bansal, and Q. Zhu, "Breast tumor characterization via complex natural resonances," *IEEE Microw. Symp. Dig.*, 387–390, June 2003.
32. Gustav, M., *Ann. Phys.*, Vol. 330, 377–445, 1908.
33. Ruck, G. T., D. E. Barrick, W. D. Stuart, and C. K. Krichbaum, *Radar Cross Section Handbook*, Vol. I, Plenum Press, New York, 1970.
34. Goodrich, R. F., B. A. Harrison, R. E. Kleinman, and T. B. A. Senior, "Studies in radar cross sections XLVII diffraction and scattering by regular bodies — I: The sphere," Radiation Lab, University of Michigan, December 1961.
35. Lee, J. W., H. J. Eom, and J. H. Lee, "TM-wave radiation from flanged parallel-plate into dielectric slab," *IEE Proc. - Microw. Antennas Propag.*, Vol. 143, No. 3, June 1996
36. Bracewell, R., *The Fourier Transform and Its Applications*, 3rd edition, McGraw-Hill, New York, 1999.
37. Kreyzsig, E., *Advanced Engineering Mathematics*, 8th edition, John Wiley & Sons, Inc., 1999.
38. Zhao, J. X., "Numerical and analytical formulizations of the

extend Mie theory for solving the sphere scattering problem," *Journal of Electromagnetic Waves and Applications*, Vol. 20, No. 7, 967–983, 2006.

39. McNamara, D. A., C. W. I. Pistorius, and J. A. G. Malherbe, *Introduction to the Uniform Geometrical Theory of Diffraction*, Artect House, Boston, 1990.
40. Jiang, L. and S. Y. Tan, "A simple analytical path loss model for urban cellular communication systems," *Journal of Electromagnetic Waves and Applications*, Vol. 18, No. 8, 1017–1032, 2004.
41. Bindu, G., A. Lonappan, V. Thomas, C. K. Aanandan, and K. T. Mathew, "Dielectric studies of corn syrup for applications in microwave breast imaging," *Progress In Electromagnetics Research*, PIER 59, 175–186, 2006.
42. Zainud-Deen, S. H., W. M. Hassen, E. M. Ali, K. H. Awadalla, and H. A. Sharshar, "Breast cancer detection using a hybrid finite difference frequency domain and particle swarm optimization techniques," *Progress In Electromagnetics Research B*, Vol. 3, 35–46, 2008.
43. Lazenik, M., L. McCartney, D. Popovic, C. B. Watkins, M. J. Lindstrom, J. Harter, S. Sewall, A. Magliocco, J. H. Booske, M. Okoniewski, and S. C. Hagness, "A large-scale study of the ultrawideband microwave dielectric properties of normal breast tissue obtained from reduction surgeries," *Phys. Med. Biol.*, Vol. 52, No. 10, 2637–2656, May 2007.
44. Lazenik, M., D. Popovic, L. McCartney, C. B. Watkins, M. J. Lindstrom, J. Harter, S. Sewall, T. Ogilvie, A. Magliocco, T. M. Breslin, W. Temple, D. Mew, J. H. Booske, M. Okoniewski, and S. C. Hagness, "A large-scale study of the ultrawideband microwave dielectric properties of normal breast tissue obtained from cancer surgeries," *Phys. Med. Biol.*, Vol. 52, No. 10, 6093–6115, October 2007.
45. Lazenik, M., M. Okoniewski, J. H. Booske, and S. C. Hagness, "Highly accurate debye models for normal and malignant breast tissue dielectric properties at microwave frequencies," *IEEE Microw. Wireless Comp. Lett.*, Vol. 17, No. 12, 822–824, December 2007.
46. Li, Y. L., "Scattering field for the ellipsoidal targets irradiated by an electromagnetic wave with arbitrary polarizing and propagating direction," *Progress In Electromagnetics Research Letters*, Vol. 1, 221–235, 2008.
47. Frezza, F., "A CWA-based detection procedure of a perfectly-

conducting cylinder buried in a dielectric half-space," *Progress In Electromagnetics Research B*, Vol. 7, 265–280, 2008.

48. Zainud-Deen, S. H., M. E. Badr, E. El-Deen, K. H. Awadalla, and H. A. Sharshar, "Microstrip antenna with defected ground plane structure as a sensor for landmines detection," *Progress In Electromagnetics Research B*, Vol. 4, 27–39, 2008.
49. Van den Bosch, I., S. Lambot, M. Acheroy, I. Huynen, and P. Druyts, "Accurate and efficient modeling of monostatic GPR signal of dielectric targets buried in stratified media," *Journal of Electromagnetic Waves and Applications*, Vol. 20, No. 3, 283–290, 2006.